ELSEVIER

Colloids and Surfaces
A: Physicochemical and Engineering Aspects 187–188 (2001) 11–21

COLLOIDS AND SURFACES A

www.elsevier.nl/locate/colsurfa

Characterization of nanoporous materials from adsorption and desorption isotherms

Peter I. Ravikovitch, Alexander V. Neimark *

Center for Modeling and Characterization of Nanoporous Materials, TRI/Princeton, 601 Prospect Ave, Princeton, NJ 08542-0625, USA

Abstract

We present a consistent method for calculation of pore size distributions in nanoporous materials from adsorption and desorption isotherms, which form the hysteresis loop H1 by the IUPAC classification. The method is based on the nonlocal density functional theory (NLDFT) of capillary condensation hysteresis in cylindrical pores. It is implemented for the nitrogen and argon sorption at their boiling temperatures. Using examples of MCM-41 type and SBA-15 siliceous materials, it is shown that the method gives the consonant pore size distributions calculated independently from the adsorption and desorption branches of the sorption isotherm. The pore size distributions, pore volumes and specific surface areas calculated from nitrogen and argon data are consistent. In the case of SBA-15 materials, the method evaluates also the amount of microporosity. The results of the NLDFT method are in agreement with independent estimates of pore sizes in regular nanoporous materials.

Keywords: Adsorption; Capillary condensation; Hysteresis; Pore size distribution; MCM-41; SBA-15; Density functional theory; Microporosity; Nitrogen; Argon

1. Introduction

Capillary condensation isotherms of vapors are widely used for calculations of pore size distributions (PSD) in nanoporous materials [1]. However, the standard methods for PSD calculations, such as the Barrett–Joiner–Halenda (BJH) method [2], are based on a simplified macroscopic description of the capillary condensation [3], which limitations at the nanoscale were repeatedly discussed in the literature [4–11]. Albeit extensive theoretical studies of the confined fluids (see [12–14] for reviews), the lack of porous solids with well-defined structures hampered the direct assessment of the accuracy of the adsorption models and, consequently, the methods for PSD analysis.

Recent progress in synthesis of nanoporous materials [15–18] lead to the development of adsorbents with highly uniform morphologies. The unique structure of MCM-41 and related materials with cylindrical pores of controlled size provides a long-desired opportunity for testing the theoretical models of capillary condensation

* Corresponding author.
E-mail addresses: ravikovi@triprinceton.org (P.I. Ravikovitch), aneimark@triprinceton.org (A.V. Neimark).

0927-7757/01/$ - see front matter
PII: S0927-7757(01)00614-8

against reliable experiments [10,19–22]. Experimental studies with mesoporous molecular sieves highlighted severe limitations of the standard methods for nanopore structure analysis, and prompted the development of new models and characterization methods [10,11,20,23–31].

In this work, we focus on the theoretical description of the capillary condensation in nanoporous materials using nonlocal density functional theory (NLDFT). Adsorption–desorption hysteresis presents another well-known problem for the PSD analysis from experimental isotherms. Which branch of the experimental adsorption–desorption isotherm should be taken for PSD calculations? Here, we present a consistent method for PSD calculations in nanoporous materials from adsorption and desorption isotherms, which form the hysteresis loop H1 by the IUPAC classification [1]. The method is implemented for N_2 adsorption at 77.4 K and for Ar adsorption at 87.3 K. The method is validated using experimental data on MCM-41 type and SBA-15 siliceous materials. The paper is organized as follows. In Section 2, we give a short description of the NLDFT model and discuss the correlations between the theoretical and experimental isotherms. In Section 3, we describe the method for PSD calculations with a special emphasis on the construction of the kernel of theoretical isotherms. In Section 4, we present several examples of PSD calculations and compare the NLDFT model with other methods. In Section 5, we offer recommendations on the application of the developed method to the PSD analysis from experimental adsorption and desorption isotherms.

2. Nonlocal density functional theory (NLDFT) of adsorption–desorption hysteresis in cylindrical pores

2.1. Model

In the density functional theory [32], the local density, $\rho(r)$, of the adsorbate confined in a pore at a chemical potential, μ, and temperature, T, is calculated by minimization of the grand thermodynamic potential, Ω:

$$\Omega[\rho(r)] = F_{\mathrm{HS}}[\rho(r)] + \frac{1}{2}\int\int \mathrm{d}r\,\mathrm{d}r'\rho(r)\rho(r')\Phi_{\mathrm{attr}}(|r-r'|) - \int \mathrm{d}r\rho(r)[\mu - U_{\mathrm{ext}}(r)] \quad (1)$$

To model the N_2 and Ar adsorption–desorption isotherms in cylindrical pores, we employed Tarazona's version of the nonlocal density functional [33], $F_{\mathrm{HS}}[\rho(r)]$, and Weeks–Chandler–Andersen [34] treatment of attractive interactions, $\Phi_{\mathrm{attr}}(r)$. We assume that $U_{\mathrm{ext}}(r)$ refers mostly to the interactions of fluid molecules with the external cylindrical layer of oxygen atoms of the pore wall [35]. A detailed description of the theory can be found in our earlier publications [10,20,23]. The fluid–fluid interaction parameters were determined from the bulk equilibrium data, the interfacial tension included [20]. The parameters of solid–fluid interactions were determined from the fit to the standard isotherms on nonporous oxides [23,36,37].

The excess adsorption per unit area of a cylindrical pore is calculated from the density distribution $\rho(r)$:

$$N_{\mathrm{s}}(P/P_0) = \frac{2}{D}\int_0^{D/2}\rho(r)r\,\mathrm{d}r - \frac{D_{\mathrm{in}}}{4}\rho_{\mathrm{g}}(P/P_0) \quad (2)$$

Here, $\rho_{\mathrm{g}}(P/P_0)$ is the bulk gas density at a given relative pressure, P/P_0; $D_{\mathrm{in}} = D - \sigma_{\mathrm{ss}}$ is the 'internal' pore diameter, which is the diameter of the cylindrical layer formed by the centers of oxygen atoms in the pore wall, D, less the effective diameter of oxygen, σ_{ss}.

2.2. Properties of adsorption–desorption isotherms in cylindrical pores. Comparison of NLDFT with experiments

The NLDFT model predicts that in the region of capillary condensation hysteresis, there are two solutions for the density distribution, $\rho(r)$, which correspond to the local minima of the grand potential. One of these solutions is a low-density, *vaporlike* state, while the other solution is a high-density, *liquidlike* state. The *equilibrium transition* corresponds to the conditions at which the grand potentials of the vaporlike and liquidlike states are equal. Within the hysteresis region, the solu-

tion with a smaller grand potential corresponds to the *stable* branch of the isotherm, while the other corresponds to the *metastable* branch. Above the equilibrium transition pressure, the vaporlike states on the adsorption branch are metastable with respect to the equilibrium liquidlike configurations on the desorption branch. The adsorption branch terminates at the vaporlike *spinodal*, where the limit of stability of metastable states is achieved and the fluid condenses spontaneously.

This is illustrated in Fig. 1, where we present the NLDFT isotherms of Ar at 87.3 K in cylindrical siliceous pores of different sizes in comparison with the experimental adsorption–desorption isotherms. The theoretical hysteresis loops shown in Fig. 1 are bounded by the lines of equilibrium transition and spinodal condensation. Metastable desorption branches at pressures below the equilibrium transition are not shown. It is known, that in the open-ended cylindrical pores the metastable

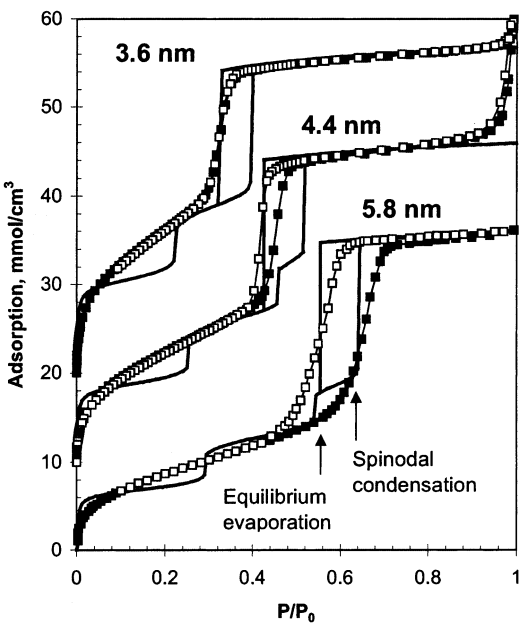

Fig. 1. Comparison of the NLDFT isotherms of Ar at 87.3 K (pore sizes are shown on the graph) with the experimental isotherms on MCM-41 [20] (pores < 5 nm), and enlarged MCM-41 material [43,44] (pores > 5 nm). Theoretical isotherms (solid lines), experimental adsorption (black squares), experimental desorption (open squares). The scale is shifted by 10 and 20 mmol cm^{-3}.

liquidlike states are not observed and the evaporation occurs at the equilibrium transition pressure [38].

By comparing the theoretical and experimental hysteresis loops, we distinguish three regimes of capillary condensation [30]. The experimental isotherms in pores smaller than the *hysteresis critical pore size* [21] are reversible and correspond to the equilibrium capillary condensation (isotherm in a 3.6 nm pore in Fig. 1). The isotherms in larger pores exhibit *developing* hysteresis loops, where the experimental desorption branch is likely to be the equilibrium one, and the experimental adsorption branch corresponds to metastable states and lies between the lines of equilibrium and spinodal transitions (isotherm in a 4.4 nm pore in Fig. 1). In pores larger than ca. 5 nm, the hysteresis loop is *developed*. The experimental desorption and adsorption branches correspond to the equilibrium and spinodal condensation transitions, respectively (isotherm in a 5.8 nm pore in Fig. 1).

Thus, the inflection point on the experimental isotherms corresponds to the theoretical equilibrium transition (reversible) pressure. For the experimental isotherms, which exhibit hysteresis, the desorption branches also correspond to the equilibrium evaporation. This is in agreement with other theories, which consider the evaporation–desorption from an open-ended single cylindrical pore as the equilibrium process [5,6,12].

A qualitatively similar picture is observed for N_2 adsorption at 77.4 K [30,37]. As an example, in Fig. 2, we present the NLDFT and the experimental isotherms for the sample of SBA-15 materials, which do not contain micropores [39]. Note that the results presented in Fig. 1 for Ar at 87 K are fully consistent with the results obtained for N_2 adsorption at 77 K on the same materials [30,40]. There are no adjustable parameters involved. Good agreement with the experimental data is achieved by tuning the parameters of intermolecular interactions to describe the equilibrium bulk thermodynamic data and adsorption on a nonporous surface. The NLDFT isotherms and hysteresis loops are also in quantitative agreement with recent Monte Carlo simulations of the same system [30].

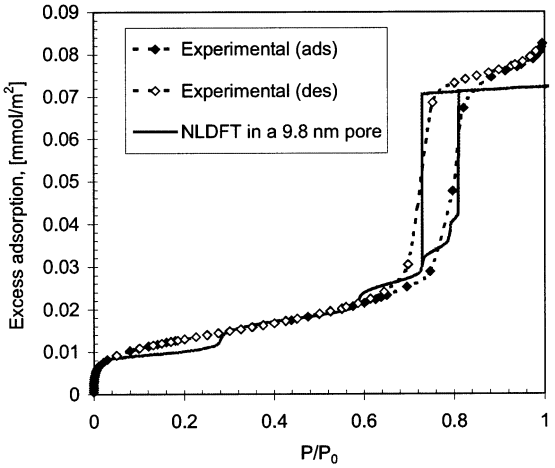

Fig. 2. Nitrogen adsorption at 77.4 K on SBA-15 material [39]. NLDFT calculations in a 9.8 nm (28 σ_{ff}) cylindrical pore (solid line).

The comparison of the theoretical and experimental isotherms shows that the calculations correctly reproduce the thickness of the multilayer adsorption film in pores of different sizes and the total amount adsorbed (Fig. 1 and Fig. 2). The step-wise behavior of the theoretical adsorption isotherms prior to capillary condensation step is attributed to the simplifications of the theoretical model, which implies a structureless model of the pore-fluid potential.

3. The NLDFT method for pore size distribution calculations from adsorption and desorption isotherms

To calculate the pore size distributions, the experimental isotherm was represented as a combination of theoretical isotherms in individual pores, which is described by the Integral Adsorption Equation (IAE) [1]:

$$N_{\mathrm{exp}}(P/P_0) = \int_{D_{\mathrm{min}}}^{D_{\mathrm{max}}} N_{\mathrm{V}}^{\mathrm{ex}}(D_{\mathrm{in}}, P/P_0)\varphi_{\mathrm{V}}(D_{\mathrm{in}})\mathrm{d}D_{\mathrm{in}} \quad (3)$$

where $N_{\mathrm{V}}^{\mathrm{ex}}(D^{\mathrm{in}}, P/P_0)$ is a kernel of the theoretical isotherms in pores of different diameters, $\varphi_{\mathrm{V}}(D_{\mathrm{in}})$ is the pore size distribution function.

3.1. Kernels

The integral (Eq. (3)) was discretized on 108 pore sizes chosen to be distributed logarithmically in the range from 1.8 to 78 nm. Two kernels of theoretical isotherms, adsorption and desorption, were calculated. Each isotherm consisted of ca. 380 pressure points to cover the range of relative pressures from 1×10^{-5} to 1. The desorption kernel consists of the equilibrium isotherms; the adsorption kernel consists of the metastable adsorption isotherms. These kernels were employed for calculating the pore size distributions from the experimental desorption and adsorption branches, respectively.

To represent the adsorption isotherms at pressures below the capillary condensation–evaporation step it is convenient to use a smooth standard isotherm, which reflects better the experimental data. The use of smooth isotherms in the multilayer adsorption region overcomes limitations of the structureless model of pore walls and simplifies the solution of the IAE (3). We have tested that this substitution does not appreciably affect the calculated pore size. The most straightforward approach would be to use a reference isotherm on a well-characterized MCM-41 material. However, an examination of the isotherms in cylindrical pores shows that adsorption per unit of pore area is enhanced as the pore size decreases due to the increased fluid-wall attraction interactions. This is evident from the NLDFT isotherms presented in Fig. 1. The steps corresponding to the formation of the second and third adsorption layers shift to lower relative pressures in smaller pores. A heterogeneous model of the solid–fluid interactions would predict smooth isotherms with the increased amount adsorbed per unit area [24,41]. On the other hand, there is a well-established experimental observation that the experimental isotherms on nanoporous materials of MCM-41 type reduced per unit of pore area are similar to each other in the mono- and multi-layer adsorption region [19,11,23]. It is reasonable to assume that adsorption per unit area scales with the pore size. To find the dependence, we adopted an approach, which utilizes a series of good quality reference MCM-41-type materials [20]. The pore

sizes were determined from the inflection point of the isotherm, and the pore volumes and the surface areas were determined by normalizing the experimental isotherm to coincide with the theoretical one within the pressure region above the capillary condensation step. As a first approximation, the enhancement of adsorption in pores over the standard isotherm on nonporous substrate was described as $N_s(D, P)/N_{STD}(P) = k(D) = 1 + \delta/D$. It turns out that for 3–4 nm pores, typical for most MCM-41 materials, $k(D) = 1.2–1.25$. This effect is quite significant for accurate determination of the surface area.

3.2. Solution of the integral adsorption equation

In general, solution of the IAE (Eq. (3)) presents a well-known ill-posed problem, which requires some degree of regularization [42]. In most calculations, we used an original QNNLS procedure. We found that for materials with a narrow pore size distribution, for which the experimental isotherm exhibits a sharp step, the standard nonnegative least squares procedure [42] can also be used.

3.3. Calculations in the case of adsorption–desorption hysteresis

The above comparison of the theoretical and experimental isotherms suggests that in the region of the developed hysteresis both adsorption and desorption branches can be used for the PSD calculations. The kernel of equilibrium capillary condensation isotherms has to be applied for calculations from the desorption branches of the experimental isotherms. The kernel of metastable adsorption isotherms has to be applied for calculations from the experimental adsorption branches. In the regime of developing hysteresis, calculations from the adsorption branch are hampered due to the lack of adequate theoretical description of the capillary condensation in this regime. The PSD has to be calculated from the desorption branch.

Fig. 3 presents the relative pressures of the equilibrium and spinodal capillary condensations as a function of the pore diameter. This plot is useful for identifying the different hysteresis regimes and selecting the most appropriate strategy for the PSD calculations. Comparison of the theoretical and experimental 'widths' of the hysteresis loops can be used for qualitative analysis of the shape of pores and the pore structure regularity. Hysteresis loops that are wider than those predicted theoretically indicate that the structure cannot be modeled as an array of independent cylindrical pores.

4. Examples. Characterization of enlarged MCM-41 and SBA-15 siliceous nanoporous materials

4.1. NLDFT pore size distribution calculations from adsorption and desorption branches

Fig. 4 presents a prominent example of PSD calculations for the MCM-41-like material [43], for which the isotherms exhibit H1 hysteresis loop. Calculations were performed from N2 and Ar adsorption and desorption isotherms. Good

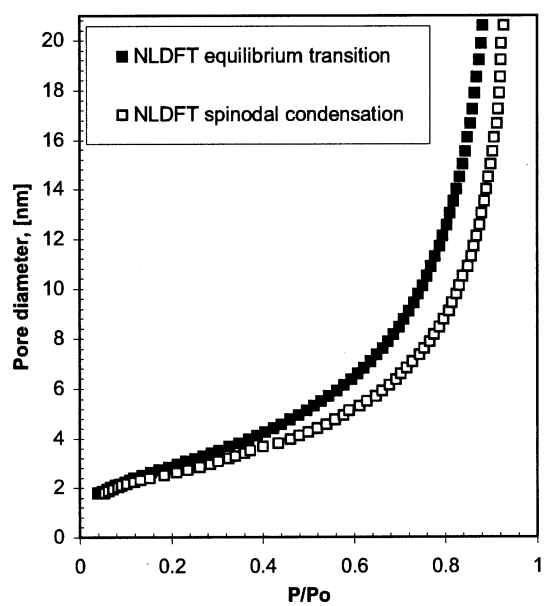

Fig. 3. Relative pressures of the equilibrium evaporation (black squares) and spinodal capillary condensation (open squares) transitions for Ar at 87.3 K in cylindrical pores of siliceous materials as calculated by the NLDFT.

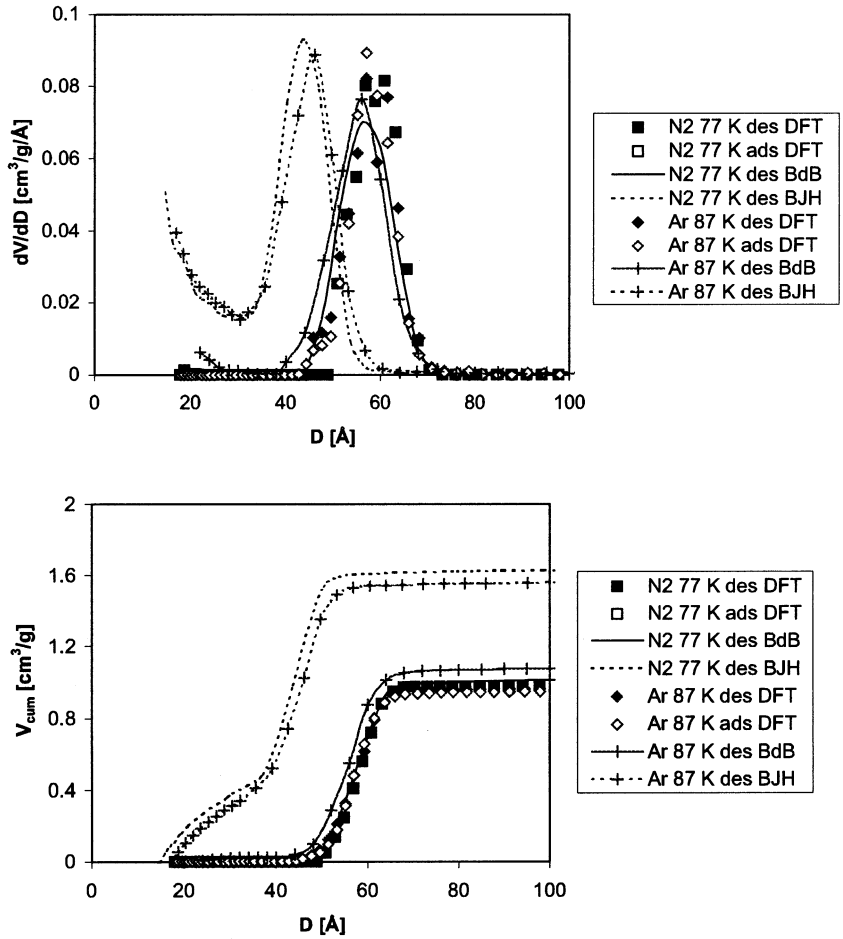

Fig. 4. Differential (top) and cumulative (bottom) pore volume distributions of enlarged MCM-41-type material [43,44] calculated from the adsorption (open symbols) and desorption (closed symbols) branches of N_2 (squares) and Ar (rhombs) isotherms. Solid and dotted lines show PSDs obtained by the BdB [5] and BJH [2] methods, respectively.

agreement between the results obtained from two gases and two branches of the isotherms is evident from the differential (Fig. 4 top) and cumulative PSDs (Fig. 4 bottom). The fit of the experimental isotherms is presented in Fig. 5.

4.2. Comparison with the macroscopic methods of PSD analysis

In our earlier publications it has been shown that the BJH method [2], which is based on the Kelvin–Cohan equation [3], becomes inaccurate for pores as large as 20 nm [40]. In materials with 2–4 nm pores, the BJH method underestimates the pore size by ca.1 nm [11], yielding unrealistically high estimates for the pore wall thickness in MCM-41 materials [20]. The methods which take into account the influence of surface forces on the thin adsorbed films [4–6], e.g. the Derjaguin-Broekhoff-de Boer (DBdB) method [5], are more accurate than the BJH method, however the deviations from the NLDFT method are significant in pores < 7 nm, especially for the adsorption branch [40].

Fig. 4 shows PSDs obtained from the BJH and DBdB methods. The parameters used were de-

scribed earlier [40]. For clarity, only calculations from the desorption branches are presented. It is seen that the BJH method significantly underestimates the pore size, by almost 1.5 nm, and overestimates the total pore volume.

4.3. Pore size distributions of SBA-15 materials. Account for microporosity

In Fig. 6, we present the N_2 adsorption–desorption isotherms on several SBA-15 materials [39]. The isotherms form H1 hysteresis loops. The pore size distributions calculated by the NLDFT methods from the adsorption and desorption branches are presented in Fig. 7. The distributions obtained from the adsorption and desorption branches are in good agreement for all samples. It is evident from the PSDs that in addition to primary channels of 5–12 nm, SBA and Al-SBA samples contain significant amounts of micropores and narrower mesopores. This is consistent with the isotherms on these samples (Fig. 6), which show that the ratio of the amount adsorbed before the capillary condensation–evaporation steps to the total amount adsorbed is larger than for the corresponding ideal cylindrical pores with smooth walls. Microporosity and roughness of the pore walls in SBA-15 are the most likely cause of this behavior, which appears to be typical for most of the SBA-15 materials [18,29,39,45]. Note, that the SBA-B sample, prepared in a basic media, does not contain micropores [39]. The isotherm on this sample agrees nicely with the theoretical isotherm calculated for a typical cylindrical pore (see Fig. 2).

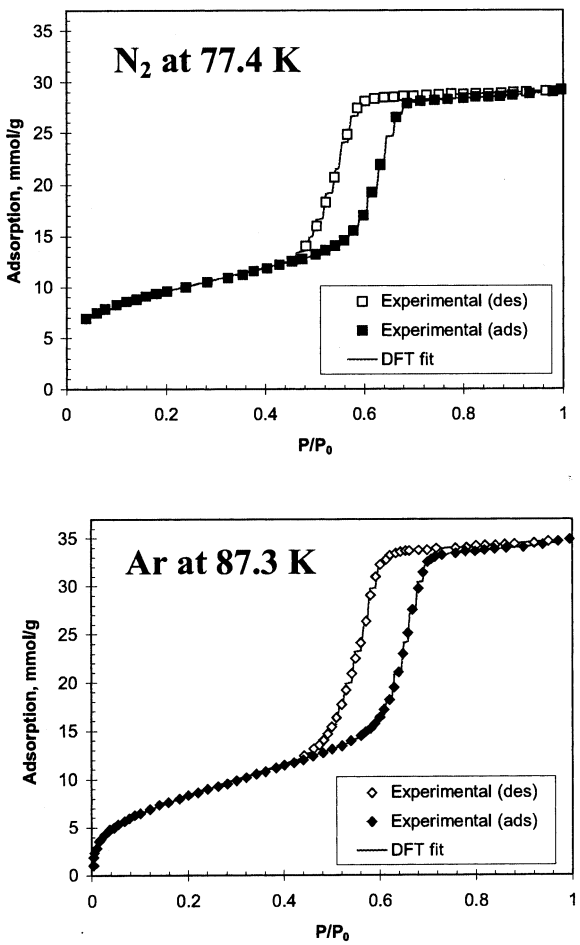

Fig. 5. NLDFT fit of the experimental adsorption and desorption isotherms of N_2 (top) and Ar (bottom) on the enlarged MCM-41-type material [43,44].

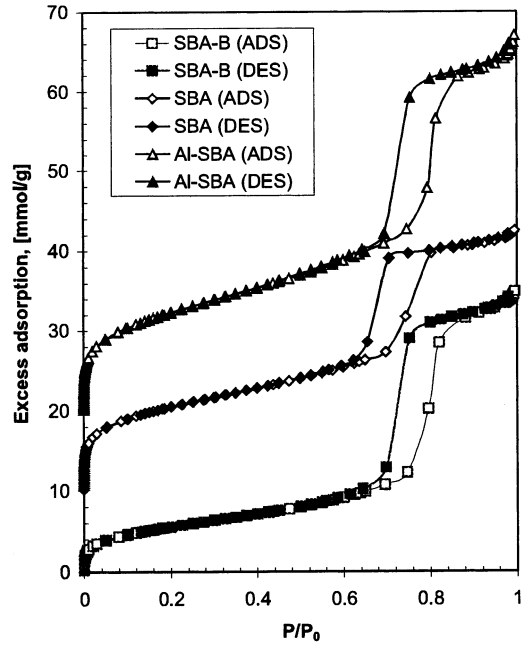

Fig. 6. Nitrogen adsorption at 77.4 K on SBA-15 materials [39]. The scale is shifted by 10 and 20 mmol g^{-1}.

4.4. Comparison with independent methods

The pore diameter of high-quality materials with hexagonal symmetry can be calculated from geometrical considerations [46,25,28] as $D_{cyl} = (\sqrt{2\sqrt{3}/\pi})a_0\sqrt{\varepsilon} \approx 1.05a_0\sqrt{\varepsilon}$, where a_0 is the lattice constant, $\varepsilon = \rho_s V_{meso}/(1 + \rho_s V_{micro} + \rho_s V_{meso})$ is the volume fraction of regular mesopores, since in general, the sample may contain micropores in addition to mesopores; V_{meso} and V_{micro} are the specific pore volumes of meso- and micro-pores, evaluated from the adsorption data; ρ_s is the density of amorphous silica. The latter parameter is usually taken as the density of amorphous silica (2.2 g cm^{-3}), however, it should be verified by helium density measurements. This approach is restricted to high-quality materials only. Another popular method is to use the $4V_{meso}/S_{meso}$ relation to evaluate the diameter of cylindrical pores from the pore volume and the surface area [47,28,29]. The latter parameter is sensitive to the method chosen for accounting for microporosity.

Although the methods based on ideal geometrical considerations are less accurate than the NLDFT method, for many high-quality materials they provide a reasonable independent estimate of the pore diameter. Fig. 8 shows how the geometrical estimates compare with the NLDFT pore sizes for a number of MCM-41 and SBA-15 materials. The plot is based on the data collected in [29], to which we added our data on MCM-41 materials [20], and literature data on enlarged MCM-41 type samples [43,44], and SBA-15 materials [39]. The volumes of micro- and mesopores in the SBA-15 materials from [39] were evaluated by the present NLDFT method from the PSD curves (Fig. 7). It is evident from Fig. 8 that for materials with pores smaller than ca. 4 nm, which show reversible adsorption isotherms, the NLDFT and 'geometrical' pore sizes generally coincide within 0.1–0.2 nm. For the materials with pores larger than 4 nm, the agreement is also good, although there is some scatter between the data on SBA-15 materials [29] and enlarged MCM-41-type materials [43,44]. It should be noted that the pore diameters taken from [29] were evaluated by the

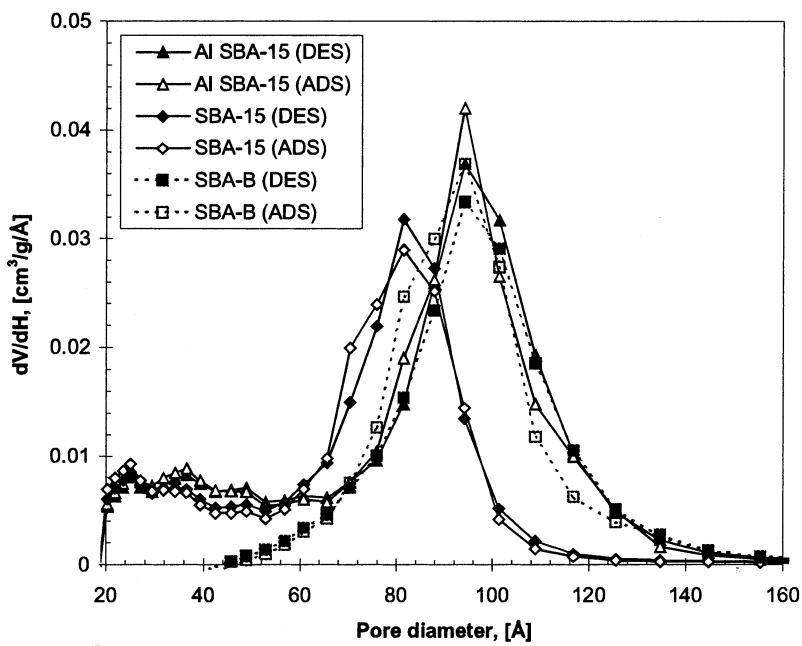

Fig. 7. The pore size distributions of SBA-15 and Al-SBA-15 materials [39] calculated from the adsorption (open symbols) and desorption (filled symbols) branches of nitrogen isotherms by the NLDFT method.

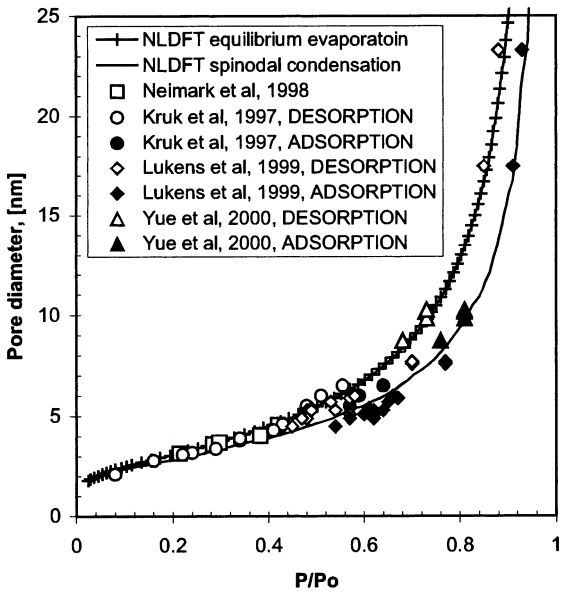

Fig. 8. Relative pressures of the NLDFT equilibrium evaporation (crosses) and spinodal condensation (solid line) for N_2 at 77.4 K in comparison with the independent experimental estimates of the pore size (points). Experimental data were taken from [20,25,29,39,43]. See text for comments.

$4V_{meso}/S_{meso}$ method. This may partially explain the observed deviations. In all cases, the widths of the adsorption–desorption hysteresis loop on the SBA-15 materials correspond well to the theoretical predictions. The observed agreement supports the NLDFT as a rational for consistent PSD calculations and evaluation of the pore volumes and surface areas.

4.5. Non-ideal systems

It should be noted that the mechanisms of capillary condensation and desorption discussed above are valid for ideal open-ended cylindrical pores. Any irregularities of the pore structure, especially the pore network effects may change this picture dramatically [1,7,48,49]. The widths of the hysteresis loops in the ideal cylindrical pores predicted theoretically in this work (Fig. 3) can be used to access significance of networking effects. The pore blocking leads to wider hysteresis loops; the desorption branch is usually very sharp compared with the adsorption branch. In this case it is reasonable to assume that the network effects affect less the adsorption branch, and to calculate PSDs from the adsorption branch using the kernel of the metastable adsorption isotherms. Calculations from the desorption branch require special network percolation methods [7,48,49], which are not considered here.

Another source of errors while using the desorption branch is related to the well-known experimental fact that desorption isotherms frequently exhibit a characteristic 'step down' at $P/P_0 \approx 0.42$ (for N_2 at 77 K). These characteristic pressures correspond to the lower limit of observable adsorption hysteresis. In this case, the step on the desorption isotherm is not associated with the evaporation from a particular group of pores, therefore calculations of pore size distributions may produce an artifact [1].

5. Conclusions and recommendations

We developed a method for consistent pore size characterization of siliceous nanoporous materials with cylindrical pores from nitrogen and argon adsorption and desorption isotherms. The kernels of equilibrium capillary condensation isotherms and the kernels of metastable adsorption isotherms of N_2 at 77 K and Ar at 87 K in individual pores (2–100 nm) were calculated by means of the nonlocal density functional theory (NLDFT). Comparison of the theoretical adsorption–desorption isotherms in cylindrical pores with the experimental isotherms can be used for a qualitative analysis of the shape of pores and the pore structure regularity. For regular structures and experimental isotherms, which form the *developed* hysteresis loop H1 by the IUPAC classification, both the adsorption and desorption branches of experimental isotherms can be used for PSD calculations. The kernel of equilibrium capillary condensation isotherms is to be applied for calculations from the desorption branches of experimental isotherms. The kernel of metastable adsorption isotherms is to be applied for calculations from the experimental adsorption branches. In the regime of *developing* hysteresis, calculations from the adsorption branch are ham-

pered due to the lack of adequate theoretical description of the capillary condensation in this regime. The PSD has to be calculated from the desorption branch using the kernel of NLDFT equilibrium isotherms. In the case of reversible capillary condensation, the kernel of NLDFT equilibrium isotherms must be used.

Using examples of MCM-41 type and SBA-15 siliceous materials, it has been shown that the NLDFT method gives the consonant pore size distributions calculated independently from the adsorption and desorption branches of sorption isotherms. The pore size distributions, pore volumes and specific surface areas calculated independently from nitrogen and argon data are consistent. In the case of SBA-15 materials, the method evaluates also the amount of microporosity. The results of the NLDFT method are in agreement with independent estimates of pore sizes in regular nanoporous materials. The NLDFT method is recommended for characterization of nanoporous materials from adsorption and desorption isotherms.

Acknowledgements

This work is supported in parts by the TRI/Princeton exploratory research program, EPA grant R825959-010, and Quantachrome Corp. We thank A. Gédéon for the table data of isotherms on SBA-15 materials.

References

[1] F. Rouquerol, J. Rouquerol, K.S.W. Sing, Adsorption by Powders and Porous Solids: Principles, Methodology and Applications, Academic Press, San Diego, 1999.
[2] E.P. Barrett, L.G. Joyner, P.H. Halenda, J. Am. Chem. Soc. 73 (1951) 373.
[3] L.H. Cohan, J. Am. Chem. Soc. 60 (1938) 433.
[4] B.V. Derjaguin, Acta Physicochim URSS 12 (1940) 181.
[5] J.C.P. Broekhoff, J.H. de Boer, J. Catalysis 9 (1967) 8.
[6] M.W. Cole, W.F. Saam, Phys. Rev. Lett. 32 (1974) 985.
[7] L.I. Kheifets, A.V. Neimark, Multiphase Processes in Porous Media, Khimia, Moscow, 1982 (in Russian).
[8] R. Evans, U.M.B. Marconi, P. Tarazona, J. Chem. Soc. Faraday Trans. 2 (82) (1986) 1763.
[9] C. Lastoskie, N. Quirke, K.E. Gubbins, in: W. Rudzinski et al. (Eds.), Equilibria and Dynamics of Gas Adsorption on Heterogeneous Solid Surfaces, Stud. Surf. Sci. Catal. 104 (1997) 745.
[10] P.I. Ravikovitch, S.C. Ó Domhnaill, A.V. Neimark, F. Schüth, K.K. Unger, Langmuir 11 (1995) 4765.
[11] P.I. Ravikovitch, D. Wei, W.T. Chueh, G.L. Haller, A.V. Neimark, J. Phys. Chem. B 101 (1997) 3671.
[12] D.H. Everett, in: E.A. Flood (Ed.), The Solid–Gas Interface, vol. 2, Marcel Decker, New York, 1967.
[13] R. Evans, J. Phys. Condens. Matter 2 (1990) 8989.
[14] L.D. Gelb, K.E. Gubbins, R. Radhakrishnan, M. Sliwinska-Bartkowiak, Rep. Prog. Phys. 62 (1999) 1573.
[15] C.T. Kresge, M.E. Leonowicz, W.J. Roth, J.C. Vartuli, J.S. Beck, Nature 359 (1992) 710.
[16] S. Inagaki, Y. Fukushima, K. Kuroda, J. Chem. Soc. Chem. Commun. (1993) 680.
[17] Q. Huo, D.I. Margolese, G.D. Stucky, Chem. Mater. 8 (1996) 1147.
[18] D. Zhao, Q. Huo, J. Feng, B.F. Chmelka, G.D. Stucky, J. Am. Chem. Soc. 120 (1998) 6024.
[19] P.J. Branton, P.G. Hall, K.S.W. Sing, H. Reichert, F. Schüth, K.K. Unger, J. Chem. Soc. Faraday Trans. 90 (1994) 2965.
[20] A.V. Neimark, P.I. Ravikovitch, M. Grün, F. Schüth, K.K. Unger, J. Coll. Interf. Sci. 207 (1998) 159.
[21] K. Morishige, M. Shikimi, J. Chem. Phys. 108 (1998) 7821.
[22] J.P. Coulomb, N. Floquet, Y. Grillet, P.L. Llewellyn, R. Kahn, G. André, Stud. Surf. Sci. Catal. 128 (2000) 235.
[23] P.I. Ravikovitch, G.L. Haller, A.V. Neimark, Adv. Coll. Interf. Sci. 77 (1998) 203.
[24] M.W. Maddox, J.P. Olivier, K.E. Gubbins, Langmuir 13 (1997) 1737.
[25] M. Kruk, M. Jaroniec, A. Sayari, J. Phys. Chem. B 101 (1997) 583.
[26] S. Inoue, S.Y. Hanzawa, K. Kaneko, Langmuir 14 (1998) 3078.
[27] C.G. Sonwane, S.K. Bhatia, Chem. Eng. Sci. 53 (1998) 3143.
[28] A. Galarneau, D. Desplantier, R. Dutartre, F. Di Renzo, Microporous Mesoporous Mater. 27 (1999) 297.
[29] W.W. LukensJr, P. Schmidt-Winkel, D. Zhao, J. Feng, G.D. Stucky, Langmuir 15 (1999) 5403.
[30] A.V. Neimark, P.I. Ravikovitch, A. Vishnyakov, Phys. Rev. E 62 (2000) R1493.
[31] M. Miyahara, H. Kanda, T. Yoshioka, M. Okazaki, Langmuir 16 (2000) 4293.
[32] R. Evans, in: D. Henderson (Ed.), Fundamentals of Inhomogeneous Fluids, Marcel Dekker, New York, 1992 Chapter 5.
[33] P. Tarazona, U.M.B. Marconi, R. Evans, Mol. Phys. 60 (1987) 573.
[34] J.D. Weeks, D. Chandler, H.C. Andersen, J. Chem. Phys. 54 (1971) 5237.
[35] G.J. Tjatjopoulos, D.L. Feke, J.A. Mann Jr, J. Phys. Chem. 92 (1988) 4006.

[36] M.M. Dubinin, L.I. Kataeva, V.I. Ulin, Bull. Acad. Sci. USSR Chem. 26 (1977) 459.
[37] P.I. Ravikovitch, A.V. Neimark, in: A. Sayari et al. (Eds.), Nanoporous Materials II, Stud. Surf. Sci. Catal. 129 (2000) 597.
[38] A. Papadopoulou, F. van Swol, U.M.B. Marconi, J. Chem. Phys. 97 (1992) 6942.
[39] Y.-H. Yue, A. Gédéon, J.-L. Bonardet, J.B. d'Espinose, N. Melosh, J. Fraissard, Stud. Surf. Sci. Catal. 129 (2000) 209.
[40] A.V. Neimark, P.I. Ravikovitch, Microporous and Mesoporous Materials, 44–45 (2001) 697.
[41] L. Gelb, K.E. Gubbins, Langmuir 14 (1998) 2097.
[42] C.L. Lawson, R.J. Hanson, Solving Least Squares Problems, SIAM, Philadelphia, 1995.
[43] A. Sayari, P. Liu, M. Kruk, M. Jaroniec, Chem. Mater. 9 (1997) 2499.
[44] M. Kruk, M. Jaroniec, Chem. Mater. 12 (2000) 222.
[45] M. Kruk, M. Jaroniec, C.H. Ko, R. Ryoo, Chem. Mater. 12 (2000) 1961.
[46] N. Coustel, F. Di Renzo, F. Fajula, J. Chem. Soc. Chem. Commun. (1994) 967.
[47] J. Rathouský, A. Zukal, O. Franke, G. Schulz-Ekloff, J. Chem. Soc. Faraday Trans. 90 (1994) 2821.
[48] A.V. Neimark, Russ. J. Phys. Chem. 60 (1986) 1045.
[49] A.V. Neimark, in: F. Rodriguez-Reinoso et al. (Eds.), Characterization of Porous Solids II, Stud. Surf. Sci. Catal., Elsevier, Amsterdam, 1991, p. 67.